Available online at www.sciencedirect.com
ScienceDirect
Journal of Photochemistry and Photobiology A: Chemistry 190 (2007) 77–87
Journal of Photochemistry and Photobiology A:Chemistry
www.elsevier.com/locate/jphotochem

The physical properties and photoresponse of $AgIn_5S_8$ polycrystalline film electrodes fabricated by chemical bath deposition

Kong-Wei Cheng [a,*], Chao-Ming Huang [b], Guan-Ting Pan [c,d], Wen-Sheng Chang [d], Tai-Chou Lee [e], Thomas C.K. Yang [c]

[a] *Department of Chemical and Materials Engineering, Chang Gung University, Taoyuan, Taiwan*
[b] *Department of Environmental Engineering, Kun Shan University, Tainan, Taiwan*
[c] *Department of Chemical Engineering, National Taipei University of Technology, Taipei, Taiwan*
[d] *Energy and Environmental Laboratory, Industrial Technology Research Institute, Hsinchu, Taiwan*
[e] *Department of Chemical Engineering, National Chung Cheng University, ChiaYi, Taiwan*

Received 9 January 2007; accepted 15 March 2007
Available online 23 March 2007

Abstract

The $AgIn_5S_8$ polycrystalline films were grown on indium–tin-oxide-coated glass substrates by using chemical bath deposition. New procedures for the growth of $AgIn_5S_8$ films are presented. The solutions containing silver nitrate, indium nitrate, triethanolamine, ammonium nitrate and thioacetamide in acidic solution were used for the growth of $AgIn_5S_8$ film electrodes. The influences of various deposition parameters on structural, optical, and electrical performances of films have been investigated. The X-ray diffraction patterns of the samples demonstrate the presence of polycrystalline structures of $AgIn_5S_8$ phase in these films and show $AgIn_5S_8$ phase is the major crystal structure. With different substrates, the different crystal structures were obtained. The thickness, band gaps and carrier densities of these samples determined from transmittance spectra and electrochemical analysis are in the range of 647–1123 nm, 1.70–1.73 eV and 4.02×10^{14}–6.36×10^{14} cm^{-3}, respectively. The flat band potentials of these samples are located between −0.293 and −0.403 V versus normal hydrogen electrode with the Mott-Schottky measurements. The conduction bands and valance bands of films determined from flat band potentials are in the range of −0.517 to −0.618 V, and +1.213 to +1.082 V versus normal hydrogen electrode. The maximum photocurrent density of samples prepared in this study with external potential kept at 3.5 V was found to be 6.0 mA/cm^2 under the illumination with white light intensity kept at 100 mW/cm^2.

Keywords: Photoelectrodes; X-ray diffraction; Optical properties; Photocurrent density

1. Introduction

The clean energy has been attracted more and more attentions due to the energy and environmental problems. In recent years, the production of hydrogen from water with solar energy becomes one of new interesting research fields because of the requirements of clean energy. Water splitting with photoelectrochemical process has been extensively studied for a long time since the Fujishima-Honda effect, which involved an n-TiO_2 photoelectrode, was reported [1]. However, the photocatalytic activity of n-TiO_2 has been limited to ultraviolet light due to its large band gap, 3.0–3.2 eV. To improve the efficiency of water splitting, many approaches have been carried out to develop the visible-light-active photocatalysts through doping of transition metal ions such as Cr^{3+}, Cu^{2+}, Ni^{2+} or Ag^{+} [2–5]. However, the number of reported photocatalysts that were able to decompose water into hydrogen and oxygen with reasonable activity has been limited. Another research direction is the development of superior photocatalysts for photoelectrochemical applications. In recent years, the I–III–VI_2 ternary semiconductors have been receiving considerable research and production interests. The band gap lies between 0.8 and 2.0 eV, which is a good absorber for photoelectrochemical devices [6]. Cu(In,Ga)Se_2 (CIGS) solar cells have been entered the industrial applications after a few decades of research and development [7]. Alternatively, other types of ternary semiconductors, $AgInS_2$ and $AgInSe_2$ have attracted increasing attentions recently because of

* Corresponding author at: No. 259 Wen-Hwa 1st Rd., Kwei-Shan, Tao-Yuan 333, Taiwan, ROC. Tel.: +886 3 2118800 3356; fax: +886 3 2118668.
E-mail address: kwcheng@mail.cgu.edu.tw (K.-W. Cheng).

1010-6030/$ – see front matter © 2007 Elsevier B.V. All rights reserved.
doi:10.1016/j.jphotochem.2007.03.015

Table 1
The reaction parameters of chemical bath deposition for the growth of $AgIn_5S_8$ polycrystalline films in this study

Samples	Solution A					Solution B	Mixture of solutions A and B	
	0.4 M $AgNO_3$ (mL)	0.4 M $In(NO_3)_3$ (mL)	7.4 M TEA (mL)	0.4 M NH_4NO_3 (mL)	18 M H_2SO_4 (mL)	0.4 M TAA (mL)	Mole ratios of Ag/In/S	Dipping numbers
a	2.00	2.00	1.00	1.00	2.00	12.0	1:1:6	1
b	2.00	2.00	1.00	1.00	2.00	12.0	1:1:6	2
c	2.00	2.00	1.00	1.00	2.00	12.0	1:1:6	3
d	2.00	2.00	1.00	1.00	2.00	12.0	1:1:6	4
e	1.43	1.43	0.71	0.72	1.43	14.3	1:1:10	4
f	1.10	1.10	0.55	0.55	1.43	15.6	1:1:14	4

their better lattices match with heterojunction CdS and $CuInSe_2$ semiconductors [8]. Another representative phase in the ternary system I–III–VI semiconductors is In-rich compounds with the general formula I–III_5–VI_8 [9]. Both Cu- and Ag-ternary semiconductors can be grown either n- or p-type, since the conduction type depends on their intrinsic defects. Recently, Kudo and co-workers [10,11] demonstrated that $CuInS_2$, $AgInS_2$ and $AgInS_2$/$CuInS_2$/ZnS solid solutions in powder form showed apparent activity for hydrogen evolution from aqueous solutions containing sacrificial reagents SO_3^{2-} and S^{2-} under visible light irradiation. The H_2 evolution rate was reported as high as 8.2 L/h-m^2. However, the photocatalyst in powder form poses some limitations associated with the filtration to recycle the particles in engineering applications after use. From the viewpoint of industrial applications, a thin film reactor is the convenient way to collect hydrogen in the water splitting without further separation process. In order to fabricate a thin film device with a superior efficiency, it is necessary to understand the properties on these I–III–VI films. Preparations with low cost fabrication technique for I–III–VI semiconductor thin films are also important for industrial applications.

Semiconductor thin films have been prepared by a variety of deposition techniques such as thermal evaporation [12], spray pyrolysis [8], plasma sputtering deposition [13,14] and solution growth techniques [15–17]. Among these deposition techniques, chemical bath deposition (CBD) is the most viable process to obtain large area and high quality semiconductor thin films with the advantages of simple, low cost and low consumption of energy [18]. For the applications of solar energy, Ag–In–S systems have suitable band gaps to be absorbers for artificial photosynthesis, however, there are few reports about the synthesis, characterization and photoresponse with Ag–In–S systems films prepared by chemical bath deposition. In this study, the synthesis of $AgIn_5S_8$ film electrodes on ITO-coated glass substrates using chemical bath deposition were developed under acidic solutions. The $AgIn_5S_8$ film characterizations such as structural, optical, and electrical properties have been carried out by using X-ray diffraction (XRD), scanning electron microscopy (SEM), X-ray photoelectron spectroscopy (XPS), UV–vis-NIR spectrophotometer and a scanning potentiostat. The performances of photoelectrochemical response using $AgIn_5S_8$ film electrodes were also carried out in this study.

2. Experimental

2.1. Materials

Analytical grade of silver nitrate ($AgNO_3$), indium nitrate ($In(NO_3)3{\cdot}5H_2O$), thioacetamide (CH_3CSNH_2, TAA), triethanolamine ($C_6H_{15}NO_3$, TEA) and ammonium nitrate (NH_4NO_3) with the purity better than 99% were purchased from Merck Co. and Simga–Aldrich Co. Sulfuric acid (H_2SO_4) and acetone ($(CH_3)_2CO$) with the purity better than 96% were purchased from Merck Co. No further purification of these chemicals was made. Aqueous cationic and anionic solutions were prepared separately before the growth of films. Indium tin oxide (ITO)-coated glass substrates were carefully cleaned ultrasonically in acetone, deionized water and ethanol subsequently for 30 min each. Finally, the ITO-coated glass substrates were washed carefully using deionized water and blown dry with ultra-pure nitrogen gas.

2.2. Fabrication of $AgIn_5S_8$ films

In this study, the same concentration (0.4 M) of solutions for $AgNO_3$ and $In(NO_3)_3$ were mixed together in appropriate volumes to obtain Ag:In molar ratio as 1:1. The concentration of triethanolamine solution kept at 7.4 M with appropriate volumes was mixed with the solution containing Ag^+ and In^{3+} to form the silver and indium complex agents (solution A). Sulfuric acid with appropriate volumes was used to adjust the pH value of solution A in the acidic conditions. The concentration of thioacetamide solution was kept at 0.4 M to provide S^{2-} for film deposition (solution B). Then, desired amount of thioacetamide solution was added into the solution A for the growth of the films. The details of the deposition parameters are given in Table 1. Pre-clean ITO-coated glass substrates were placed vertically into the beaker containing the reaction solution. The reaction solution was put on a hot plate with magnetic stirring. In order to increase the reaction rate, the temperature of solution was kept at 80 °C. A brownish colored homogeneous layer was obtained on the ITO-coated substrate. In order to increase the film thickness, multiple dipping was carried out in a freshly prepared solution bath after a period of 30 min. The films were annealed for 1 h in tube furnace purged with Ar gas at temperatures from 500 to 600 °C after final deposition.

2.3. Characterization of $AgIn_5S_8$ films

The phase formation and crystallographic study of films were measured using an X-ray diffractometer, Model Rigaku RINT 2000, Cu Kα radiation in the 2θ-range from 20° to 70°. Scan rate was set at 3° min^{-1} in order to increase signal-to-noise ratio. The surface morphology of the films was studied using a scanning electron microscope, Model JEOL JSM 6700F. The compositions of the film surface were examined using X-ray photoelectron spectroscopy (XPS), Model VG ESCALAB 250 with Al Kα exciting the X-ray source ($h\nu$ = 1486.7 eV) at 15 kV and 100 W. All binding energies were calibrated to C 1s at 285 eV, as the hydrocarbon content present on the sample. Standard curve fitting procedure was carried out for quantitative analysis. Convolution of Gaussian and Lorentzian functions with Shirley background was utilized. The quantitative analyzes of Ag 3d, In 3d and S 2p spectra were carried out using X-ray photoelectron peak fitting program, XPSPEAK version 4.1 created by Raymund Kwok's group [19].

2.4. Electrical property measurements

Photocurrent measurements were carried out in a Pyrex electrolytic cell. The semiconductor film of $AgIn_5S_8$, a Pt plate electrode (both with an average area of 1.0 cm^2) and an Ag/AgCl electrode were employed as working, counter and reference electrodes, respectively. A Cu wire was attached to the conducting layer of working electrode with silver paste, and the back contact and edges of the working electrode were sealed with epoxy resin. The electrolyte, aqueous K_2SO_3 (0.25 M) and Na_2S (0.35 M) solution, was freshly prepared using double deionized water and degassed by purging with Argon gas (99.99% purity) before each experiment. Another electrolyte, Ar-purged aqueous K_2SO_4 (0.5 M) solution with different pH values was also employed for the measurement of Mott-Schottky plot in this study. The pH values of electrolytes were adjusted with sodium hydroxide (NaOH) and sulfuric acid (H_2SO_4). Finally, the electrolytes were put into the ultrasonic bath for 30 min before each experiment in order to decrease the gas solutes in electrolytes. Photocurrent measurements with two electrodes, which were working and counter electrodes, as a function of applied potential in the range of −1.0 to 3.5 V were carried out using a computer-controlled potentiostat (Autolab Model PGSTAT 30) for all photoelectrochemical experiments, both in dark and under illumination. The sweep rate of applied potential was set at 5 mV/s. A 300 W Xe short arc lamp (Perkin-Elmer Model PE300UV) with light intensity kept at 100 mW/cm^2 was employed to simulate the solar light in this study. The quantum efficiency under monochromatic light illumination was carried out using a monochromator (Sciencetech Model 9030) assisted by an automatic filter wheel, placed between the photoelectrochemical cell and the light source. The Mott-Schottky plot of the $AgIn_5S_8$ films was measured with standard three electrodes setup by using computer-controlled potentiostat (Autolab Model PGSTAT 30) equipped a frequency response analyzer (Autolab FRA2 modules). The mobility and carrier concentrations of the samples were also measured by room temperature Hall measurements (Model Accent HL5500PC).

2.5. Optical property measurements

The spectral transmittances of the films were measured by the normal incident double beam UV–vis-NIR spectrophotometer (Perkin-Elmer Lambda 900) in the wavelength range from 300 to 2000 nm at room temperature. The transmittance spectra of the films were measured with air as the reference. The absorptions of films were measured by placing an identical ITO-coated glass substrate as the reference. The optical properties of samples in this study were obtained using transmittance spectra and data regression.

3. Results and discussion

The films of Ag–In–S semiconductors were grown on ITO-coated glass substrates by chemical bath deposition. While the molar ratio of Ag:In:S as 1:1:2 in reaction solution, no apparent film was obtained on the ITO-coated glass substrates. The growth mechanism of Ag–In–S ternary system films can be described from the following reactions:

$$CH_3CSNH_2 + H^+ \rightarrow H_2S + CH_3CNH^+$$

$$H_2S + H_2O \rightarrow HS^- + H_3O^+$$

$$HS^- + H_2O \rightarrow S^{2-} + H_3O^+$$

The overall reaction was given by

$$Ag^+ + (5-4x)In^{3+} + (8-6x)S^{2-} \rightarrow xAgInS_2/(1-x)AgIn_5S_8, \quad x = 0\text{–}1$$

The colors of the semiconductor films were darker with more dipping in a fresh-prepared reaction solution. These semiconductor films with various deposition parameters were analyzed such as structural, optical, and electrical properties in this study.

3.1. Crystal structure analysis

Since the ITO-coated glass substrates were damaged during high temperature thermal treatment (>600 °C), the maximum temperature of thermal treatment for Ag–In–S films was set to 600 °C. The detailed analysis of thermal treatments on the crystal structure of films was investigated in this work. Fig. 1 shows the X-ray diffraction patterns of sample f under various thermal treatment temperatures, from 500 to 600 °C. The standard diffraction peaks of $AgInS_2$ [20], $AgIn_5S_8$ [21] reported in JCPDS cards are also shown in Fig. 1. The sample f deposited on ITO-coated glass substrate was found to contain the $AgIn_5S_8$ phase. The intensities of $AgIn_5S_8$ phase increase with increasing of temperature for thermal treatments. However, the resistance of ITO-coated glass substrates with high temperature thermal treatment (600 °C) becomes three times higher than those with thermal treatment less than 550 °C using a four probe measurement.

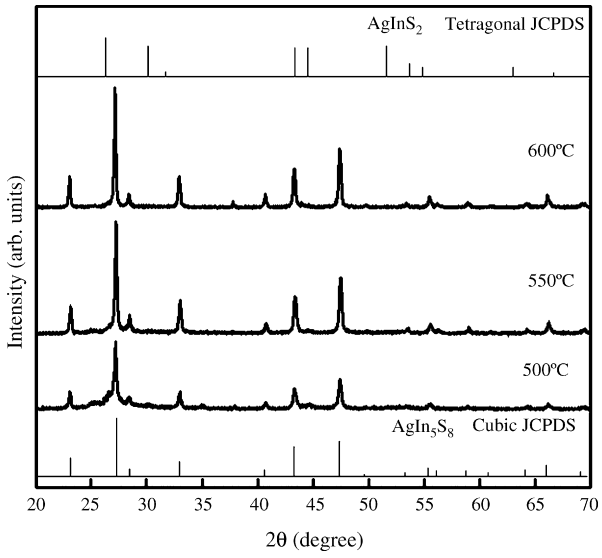

Fig. 1. X-ray diffraction patterns of sample f under various thermal treatment temperatures for 1 h.

From these experimental results, a better temperature of thermal treatment was set at 550 °C for 1 h in this study.

Fig. 2 shows the X-ray diffraction patterns of samples prepared with various reaction parameters of chemical bath deposition in this study. The X-ray diffraction patterns of samples prepared in this work show the polycrystalline structures in these films. Cubic structure of $AgIn_5S_8$ was clearly seen in samples deposited in chemical bath for one to four times. The intensities of cubic $AgIn_5S_8$ phase increase with the increasing of the dipping numbers for the films. It is interesting that the intensities of $AgInS_2$ phase appeared when the samples were immersed in a freshly prepared reaction solution for three times. The properties of substrates and solubility products for the Ag_2S and In_2S_3 compounds give the answer of these results. The solubility products of Ag_2S and In_2S_3 equals to $10^{-36.3}$ and $10^{-44.3}$, respectively [22]. Because the solubility product data of Ag_2S and In_2S_3 are very small, most of Ag^+ and In^{3+} cations in solution form the Ag_2S and In_2S_3 compounds. The solid Ag_2S and In_2S_3 compounds could be formed in powders suspended in solution or the deposited on ITO-coated glass substrates. The molar ratios of In_2S_3 compounds deposited on ITO-coated glass substrates for one and two times are higher than Ag_2S because of the interactions between ITO-coated glass substrates and the deposited compounds. Since the indium is one of the elements of ITO-coated glass substrates, the attracting force between In_2S_3 and ITO-coated glass substrates is much higher than that of Ag_2S compounds. After thermal treatment of semiconductor films, the major crystal structure of $AgIn_5S_8$ was observed in X-ray diffraction patterns. Because the molar ratio of In_2S_3 in film deposited for two times (sample b) was higher than that of Ag_2S in the films, the growth rate of In_2S_3 compounds in the film becomes a little more slower than that of Ag_2S compounds (sample c). After thermal treatment of the film on ITO-coated glass substrates, the crystal structure of $AgInS_2$ phase was observed in XRD patterns. From XRD diffraction patterns of samples prepared with the same molar ratio of S/Ag in reaction solutions (samples a–d), the intensities of cubic $AgIn_5S_8$ phase in sample d are in the highest value. Because there are more Ag_2S compounds formed in the films deposited for three times, the growth rate of In_2S_3 in the films (sample d) become faster than that deposited for three times (sample c). After thermal treatment of the film on ITO-coated glass substrates, the rearrangements of molecules and formation of more stable chemical structure, $AgIn_5S_8$ phase. With the higher molar ratio of S^{2-} species in solutions, the growth rate of Ag_2S and In_2S_3 will become faster. Since the interaction between ITO-coated glass substrates and In_2S_3 is much stronger than Ag_2S, after thermal treatment of films deposited on ITO-coated glass substrates for four times, the higher intensities of $AgIn_5S_8$ phase appeared in the XRD patterns. Fig. 3 shows the XRD patterns of samples with various reaction parameters deposited on glass substrates in this work.

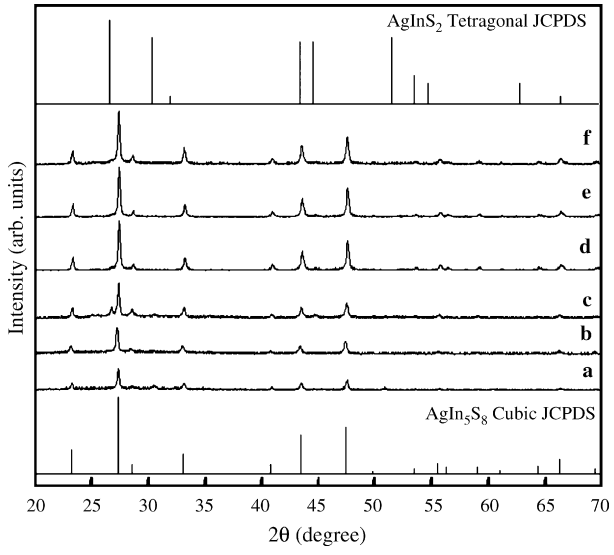

Fig. 2. X-ray diffraction patterns of the films deposited on ITO-coated glass with various reaction parameters using chemical bath deposition.

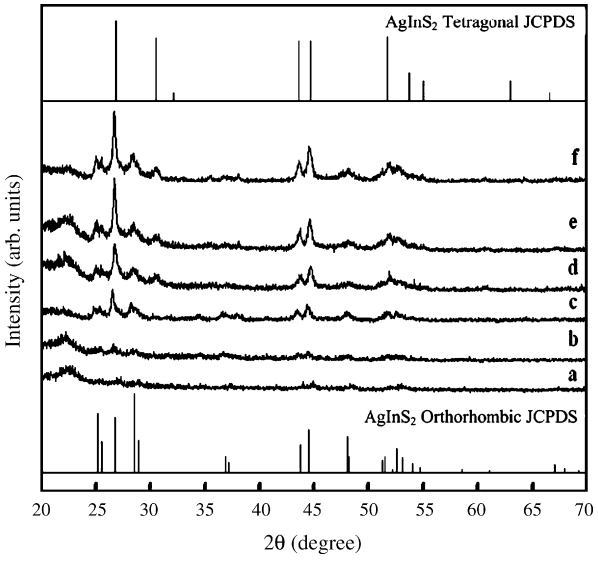

Fig. 3. X-ray diffraction patterns of films deposited on glass substrates with various reaction parameters using chemical bath deposition.

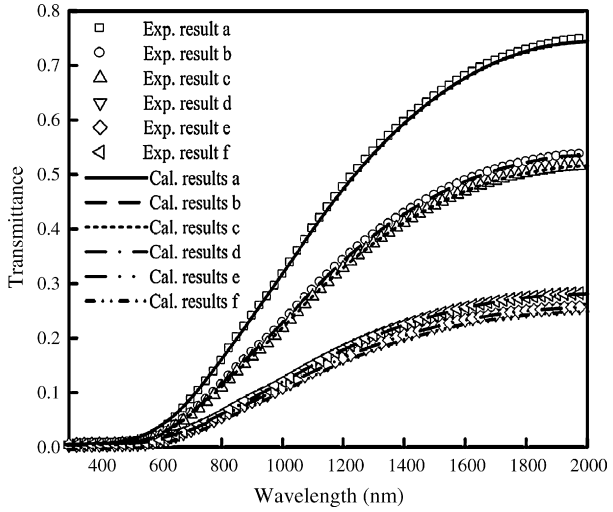

Fig. 4. Transmittance spectra of the films deposited on ITO-coated glass substrates with various reaction parameters using chemical bath deposition.

The intensities of crystal structure are much smaller than the samples deposited on ITO-coated glass substrates. The experimental results show the major crystal structures of films on glass substrates turned into tetragonal and orthorhombic $AgInS_2$ after 550 °C thermal treatment for 1 h. Because the interactions between glass substrates and Ag_2S or In_2S_3 are weaker than those between ITO-coated glass and In_2S_3, the growth rate of Ag_2S and In_2S_3 are almost the same. The $AgInS_2$ crystal structures of films on glass substrates were observed. These results confirm our explanation and indicate the interaction between films and substrates is an important factor for the formation of crystal structures.

3.2. Optical properties

The transmittance spectra of semiconductor films obtained by chemical bath deposition are shown in Fig. 4. Sample a shows transmission ca. 75%. The transmittance of sample prepared in this study decreases with the increasing dipping numbers (samples a–d). The transmittances of films on ITO-coated glass are almost the same with the increasing of molar ratio of thioacetamide (samples d–f). Energy gaps and thickness of the films deposited on substrates are two of important properties for the applications of photoelectrochemical reaction. For films having complex refractive index, $N = n - ik$, on a thick substrate ($N = n_s$), thickness and optical constants of films can be calculated from transmittance spectra with data regression. Many formulas have been proposed to describe the transmittance spectra of film on the transparent substrates [23–25]. In this study, the transmittance spectra of films grown on ITO-coated glass were fitted using the following formula [25]:

$$T = \frac{64n_0^2 n_s^2 (n^2 + k^2)}{a_1 \exp(b) + a_2 \exp(-b)} \tag{1}$$

$$a_1 = 2\{(n_0 + n)^2 + k^2\}\{(n_s^2 + n_0^2)(n_s^2 + n^2 + k^2) + (4nn_0 n_s^2)\} \tag{2}$$

$$a_2 = 2\{(n_0 - n)^2 + k^2\}\{(n_s^2 + n_0^2)(n_s^2 + n^2 + k^2) - (4nn_0 n_s^2)\} \tag{3}$$

$$b = \frac{4\pi k \mathrm{d}}{\lambda} = \alpha d \tag{4}$$

where n, k, α and d are the refractive index, extinction coefficient, absorption coefficient and thickness of film, respectively. n_0 and n_s are the refractive indices of air and substrate. For simplicity, it has been assumed that optical losses due to scattering and effect of back surface reflections from substrate are negligible.

The dispersion of optical constants for various materials has been studied by many authors. Different dispersion equations of $n(\lambda)$ and $k(\lambda)$ have been proposed to characterize the optical properties of films. Forouhi and Bloomer [26] proposed the dispersion equations for n and k that satisfy Kramers–Kronig relation. The quantum theory for electron transitions was employed to drive dispersion equations and applied them to fit the data for a wide class of amorphous dielectrics and semiconductors. The Forouhi dispersion equations are:

$$n(E) = n(\infty) + \sum_{i=1}^{q} \frac{B_{0,i}E + C_{0,j}}{E^2 - B_i E + C_i} \tag{5}$$

$$k(E) = \sum_{i=1}^{q} \frac{A_i (E - E_g)^2}{E^2 - B_i E + C_i} \quad \text{for } E > E_g$$
$$k(E) = 0 \quad \text{for } E < E_g \tag{6}$$

where E is the photon energy, E_g the optical energy bandgap, A–C and $n(\infty)$ are the independent parameters. B_0 and C_0 are related to the independent parameters as follows:

$$B_{0,i} = \frac{A_i}{Q_i}\left(-\frac{B_i^2}{2} + E_g B_i - E_g^2 + C_i\right) \tag{7}$$

$$C_{0,i} = \frac{A_i}{Q_i}\left[(E_g^2 + C_i)\left(\frac{B_i}{2}\right) - 2E_g C_i\right] \tag{8}$$

$$Q_i = \frac{1}{2}(4C_i - B_i^2)^{1/2} \tag{9}$$

where $4C_i - B_i^2 > 0$. The n_s takes as a function of wavelength with the power series wavelength-dependent form and was obtained by fitting the transmittance spectrum of ITO-coated glass substrate. The dispersion equation of Forouhi and Bloomer was employed for the calculation of optical constants for the films. In this study, it is assumed that it is possible to regress experimental transmittance data by using one term ($q = 1$) of Forouhi and Bloomer equation. The refractive index, n, extinction coefficient, k, and thickness of film d can be obtained by fitting experimental transmittance spectra with iterative methods. The object function is minimized:

$$\text{obj} = \frac{100}{L}\sum_{i=1}^{L} \frac{|T_{\text{cal},i} - T_{\text{exp},i}|}{T_{\text{exp},i}} \tag{9'}$$

where L is the number of transmittance spectra data. Table 2 shows the values of dispersion equations parameters obtained

Table 2
Calculated results of transmittance spectra for the $AgIn_5S_8$ polycrystalline films using Forouhi-Bloomer dispersion equation.

Samples	Forouhi-Bloomer dispersion equation						
	A	B (eV)	C(eV^2)	$n(\infty)$	E_g (eV)	d (nm)	AAD (%)[a]
a	6.27	1.67	0.64	1.37	1.73	647	2.52
b	6.34	1.86	0.38	1.04	1.72	723	2.62
c	6.46	1.92	0.24	0.84	1.72	788	2.54
d	6.52	1.95	0.18	0.81	1.71	792	2.43
e	6.69	1.97	0.15	0.75	1.71	811	2.18
f	6.87	2.03	0.09	0.72	1.70	1123	2.04

[a] $AAD(\%) = 100/L\sum_{i=1}^{L}|T_{cal,i} - T_{exp,i}|/T_{exp,i}$.

from the regression of transmittance spectra and absolute average deviations (AAD) of transmittance spectra for $AgIn_5S_8$ polycrystalline films on ITO-coated glass substrates. Fig. 4 shows the calculated results using Forouhi and Bloomer dispersion equation and formula of transmittance spectra for Eq. (1). The calculated results agreed well with experimental data of transmittance spectra for these films. It is observed that Forouhi and Bloomer dispersion equation give the good calculating results with the AAD less than 2.62% in the range from 300 to 2000 nm. The thicknesses of films at various reaction parameters obtained from Forouhi and Bloomer dispersion equations are listed in Table 2. The thicknesses of films deposited on ITO-coated glass substrates lied between 647 and 1123 nm, which increase with the increasing of dipping number and the molar ratio of thioacetamide. The thickness of film growth is not linearly dependent on the dipping number and molar ratios of thioacetamide. It could be attributed to the different growth mechanism in each step of deposition. Figs. 5 and 6 show the relations between refractive index n, extinction coefficient k and wavelength using Forouhi and Bloomer dispersion equation and formula of transmittance spectra in Eq. (1), respectively. The refractive index of samples was in the order a > b > c > d > e > f, while the extinction coefficient of samples was in the same trend.

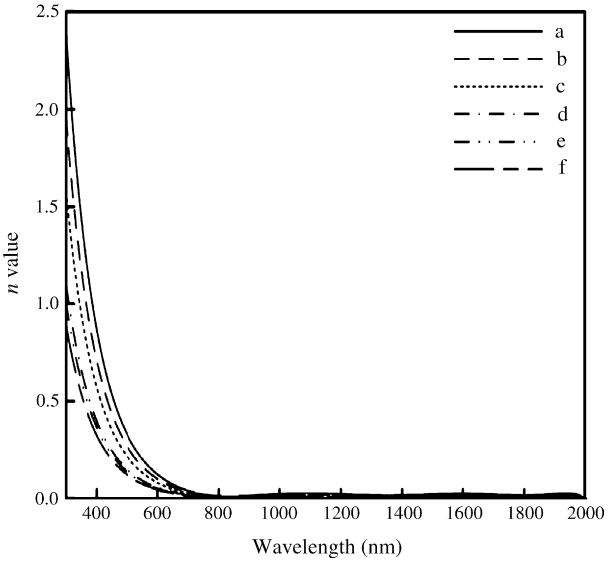

Fig. 5. The relations between refractive index n and wavelength of incident light for $AgIn_5S_8$ polycrystalline films in this study.

Both refractive index and extinction coefficient decrease with the increasing of wavelength of incident light and approach to zero with the incident light wavelength greater than 800 nm. Table 2 shows the values of band gap with different deposition parameters obtained from Forouhi and Bloomer dispersion equation and formula of transmittance spectra in Eq. (1). The band gap of $AgInS_2$ is in the range of 1.8–2.1 eV [27]. There are some reports have been published about the band gap of $AgIn_5S_8$ films. Their results show the band gap of $AgIn_5S_8$ film in the range of 1.7–1.8 eV [28–30]. The optical energy band gaps approach to 1.7 eV with the increasing of dipping numbers and the molar ratios of S/Ag. It is indicated that the major crystal structures of films approach to the $AgIn_5S_8$ phase, which agreed with the results obtained from XRD patterns. Fig. 7 shows the UV–vis-NIR absorption spectra for samples prepared in this study. The spectrum of sample a showed the absorption edge at 710 nm and the absorption shifted towards higher wavelength side with the increasing of dipping number and the molar ratios of S/Ag. The absorption edge of sample f approached to 760 nm, which agreed with the results obtained from Table 2.

3.3. Microstructure and compositional studies

Scanning electron microscope was employed to analyze the microstructure of films in this study. In general, the formation of

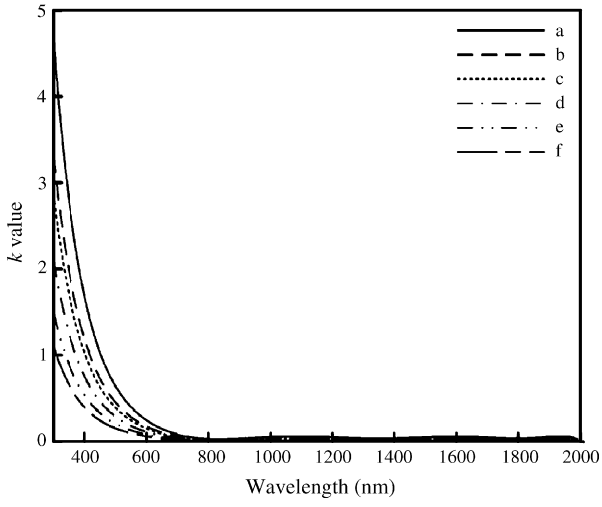

Fig. 6. The relations between extinction coefficient k and wavelength of incident light for $AgIn_5S_8$ polycrystalline films in this study.

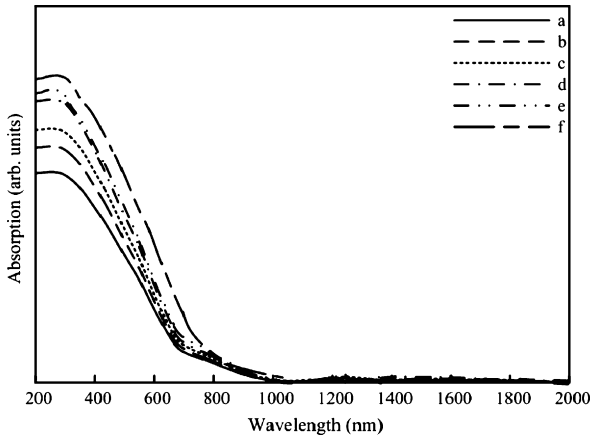

Fig. 7. UV–vis-NIR absorption spectra of $AgIn_5S_8$ polycrystalline films prepared in this study.

films using chemical bath deposition can be characterized into three schemes: (a) ion-by-ion deposition, (b) cluster-by cluster deposition and (c) mixed process. Mechanism (a) leads to smooth films, (b) appears particulate films and (c) shows colloids included in the films [31]. Most of films prepared by using chemical bath deposition are following the mixing process. Figs. 8–10 present the SEM images of samples a, d and f at 40 K (X). The diamond-like microstructures are observed for these film surfaces. The SEM image of sample d shows much more uniform morphology compared to other samples. The cracks and holes are observed on the film surface of samples a and f. From SEM images of samples a and d, it is clearly seen that grains on the film at lower reaction time are smaller in size than that of longer time. It is well known that in chemical bath deposition, thickness and grain size increase with longer deposition time. Zhai et al. [32] presented the same results for the growth of Sb_2S_3 film. From the SEM pictures of samples d and f, it is clearly seen that grains on the film at lower molar ratio of S/Ag are more uniform than that of higher molar ratio of S/Ag. In general, there are two mechanisms, which are the instantaneous (site-saturated) nucleation and constant nucleation rate for the growth of film during

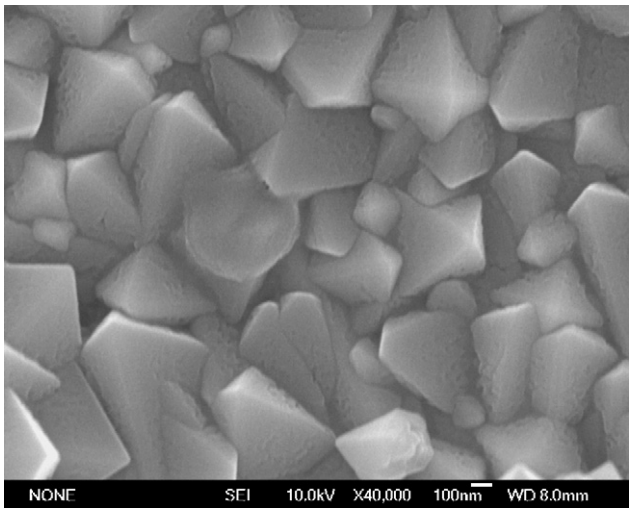

Fig. 9. The SEM image of $AgIn_5S_8$ polycrystalline films for sample d.

the reaction period [33]. For instantaneous nucleation, the substrate area is allocated the existing number of nuclei. There is no new nuclei generated on the films during the reaction period. The particles on the substrates will grow during the reaction period. For constant nucleation rate, the surface particles generation and growth occur simultaneously leading to the size distribution of particles on the films. The experimental results show three situations for the growth of films in this study. When the molar ratio of Ag:S is less than 1:6, there are not enough nuclei on the substrates. No apparent film was obtained on the ITO-coated glass substrates. The instantaneous nucleation appears when the molar ratio of Ag:S achieves 1:6. When the ratio of S/Ag is higher than 6/1, the mechanism of constant nucleation rate appears because there are a lot of nuclei formation during the reaction period. It is observed the grain size distribution on the films.

Surface compositions of samples d–f were analyzed by using an X-ray photoelectron spectrometer. The elemental compositions for the films surface of samples d–f are listed in Table 3. It is shown that the ratios of elemental compositions for samples

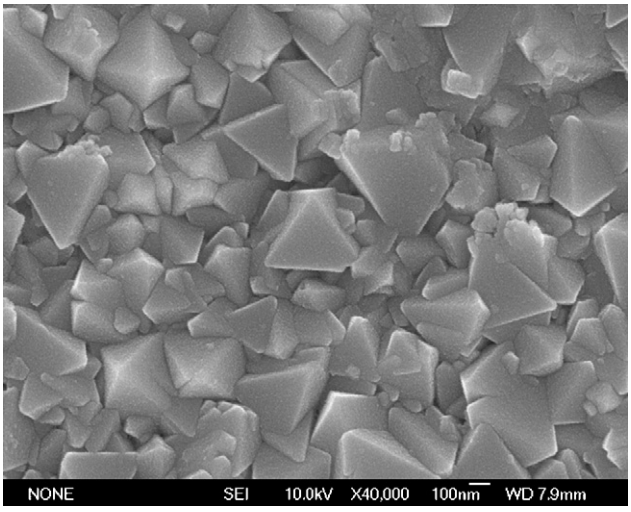

Fig. 8. The SEM image of $AgIn_5S_8$ polycrystalline films for sample a.

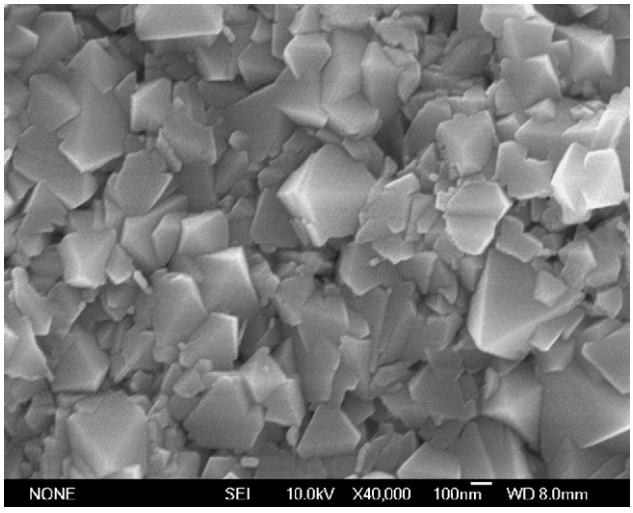

Fig. 10. The SEM image of $AgIn_5S_8$ polycrystalline films for sample f.

Table 3
The molar ratios of elements for the surface of $AgIn_5S_8$ polycrystalline films using chemical bath deposition

Sample	Mole ratios of elements for films		
	Ag	In	S
d	1.0	4.0	5.6
e	1.0	4.1	5.4
f	1.0	4.2	5.3

d–f are almost the same in this study. It indicates that the elemental compositions of the film surface of samples will achieve the stable compositions after reaction time of film growth for 2 h. The atomic ratio of [Ag]:[In]:[S] for the film surface of samples are in the range of 1:4.0–4.2:5.3–5.6. These atomic ratios indicate the $AgInS_2$ compounds formed in these films on ITO-coated glass substrates, which agreed well with the results of XRD diffraction patterns for these samples.

3.4. The electrical properties of films

The study of semiconductor/metal and semiconductor/electrolyte Schottky barrier is important in the applications of solar energy and rectification. Several methods for studying Schottky barrier have been proposed. One method based on the capacitance versus applied potential measurement is the Mott-Schottky relationship for the barrier. The Mott-Schottky equation is shown as follows:

$$\frac{1}{C^2} = B\frac{2}{\varepsilon\varepsilon_0 e N_D A^2}\left(E - E_{FB} - \frac{kT}{e}\right) \quad (10)$$

where ε is the dielectric constant of semiconductor, A the surface area of the interface, N_D the carrier density of semiconductor, E_{FB} the flat-band potential of semiconductor, which close to the potential of Fermi level for semiconductor, e the electronic charge and ε_0 is the permittivity of vacuum. For n-type semiconductor, B equal to 1, while for p-type semiconductor, B equal to -1. From this relationship, E_{FB} can be obtained from E_0, the point of intersection of a C^{-2} versus applied potential (E) plot with the E-axis:

$$E_0 = E_{FB} + \frac{kT}{e} \quad (11)$$

If, further, ε and A are known, N_D can be determined. These data then allow the determination of E_c^s or E_V^s, which are the positions of conduction and valance band for semiconductors. The dielectric constant of $AgIn_5S_8$ is 10.3 [34] and the area of interface was kept at 1 cm^2 in this work. The Mott-Schottky plots of samples at various parameters were carried out in a 0.5 M K_2SO_4 solution with pH values at 6, 8 and 10. Impendence analysis was performed on the cell by developing a physically reasonable equivalent circuit for the cell, and then fitted the measuring impendence data to this expression. For non-ideal electrode, the equivalent circuit can be complicated. Generally, for the frequency approaching to infinite, the equivalent circuit can be simplified into a series of resistance–capacitance (RC) circuit, i.e. the frequency higher than 1 kHz. In this study, the frequency of impendence was set at 1 kHz to measure Mott-Schottky plots for various samples. Fig. 11 shows the Mott-Schottky plot for the different samples. It was observed that C^{-2} versus applied potential V produces the straight lines and is almost independent on the pH of the electrolyte solution. It is known that sulfur species semiconductors do not react with H^+ or OH^- ion in solution. The band edges at the interface do not shift with the pH values of the solution. Table 4 shows the values of flat band potentials of samples at various deposition parameters. The flat band potentials of these samples prepared in this study lie in the range of -0.29 to -0.40 V versus normal hydrogen electrode (NHE). The flat band potential can also

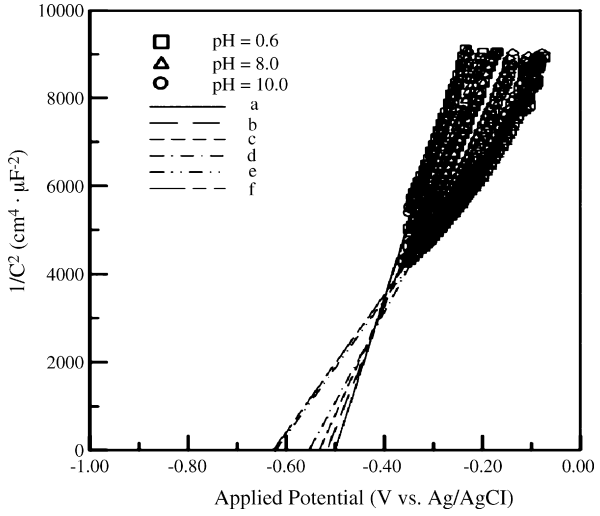

Fig. 11. Mott-Schottky plot for the samples of various reaction parameters using chemical bath deposition.

Table 4
The physical properties of $AgIn_5S_8$ polycrystalline films on ITO-coated glass substrates using chemical bath depositions

Samples	Carrier density (cm^{-3})[a]	Carrier density (cm^{-3})[b]	Mobility ($cm^2/V\,s$)[b]	E_g (eV)	E_{FB}^{NHE} (V)	E_{CB}^{NHE} (V)	E_{VB}^{NHE} (V)	E_{CB}^{Vacuum} (V)	E_{VB}^{Vacuum} (V)	Conduction type
a	4.02×10^{14}	4.05×10^{14}	0.839	1.73	−0.293	−0.517	1.213	−3.983	−5.713	n
b	4.93×10^{14}	4.34×10^{14}	0.783	1.72	−0.313	−0.532	1.188	−3.968	−5.688	n
c	4.54×10^{14}	4.52×10^{14}	0.751	1.72	−0.333	−0.554	1.166	−3.946	−5.666	n
d	5.31×10^{14}	5.29×10^{14}	0.642	1.71	−0.373	−0.590	1.120	−3.910	−5.620	n
e	6.36×10^{14}	6.33×10^{14}	0.537	1.71	−0.403	−0.616	1.094	−3.884	−5.594	n
f	5.75×10^{14}	5.76×10^{14}	0.589	1.70	−0.403	−0.618	1.082	−3.882	−5.582	n

[a] Calculated from Mott-Schottky plot.
[b] Obtained from Hall measurements.

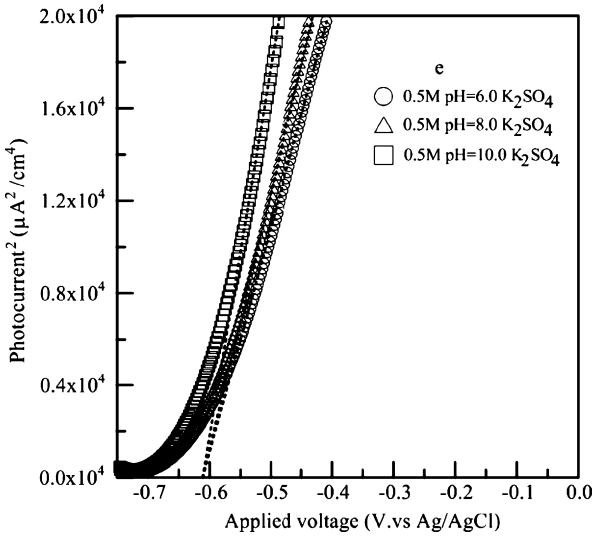

Fig. 12. The flat band potential of sample e obtained from photocurrent density^2–applied voltage plot at wavelength of incident light $\lambda = 700$ nm.

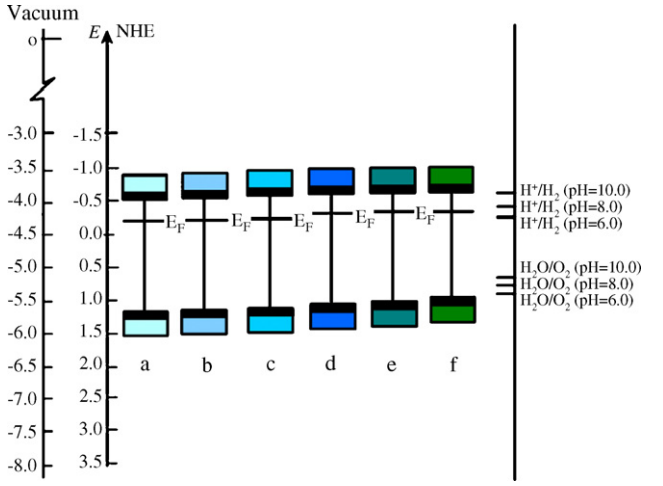

Fig. 13. Band positions of samples determined by electrochemical measurements and transmittance spectra in this study.

be determined from the relationship between monochromatic photocurrent density $I_p(\lambda)$ and the applied voltage E using the relation derived for small band bending [35]:

$$E - E_{FB} = BI_p^2(\lambda) \quad (12)$$

Fig. 12 shows a plot of $I_{p(\lambda)}{}^2$ measured at incident light wavelength kept at 700 nm versus applied voltages E for sample e. Straight lines were obtained for sample e at different pH values of 0.5 M K_2SO_4 electrolytes with the same intercept around −0.61 V versus an Ag/AgCl reference electrode (−0.403 V versus NHE), which agreed with the experimental result from Table 4. The positions of flat band potential are more negative with the increasing of dipping numbers and the molar ratio of thioacetamide. The values of carrier density of samples in this study are also present in Table 4. The values of carrier density of $AgIn_5S_8$ polycrystalline films are in the range of 4×10^{14}–6.4×10^{14} cm^{-3}, which are agreed well with those from the Hall measurement. The conduction types of these samples grown from chemical bath deposition show the n-type semiconductor. The mobility of these samples deposited on ITO-coated glass substrates lie in the range of 0.537–0.839 cm^2/V s, which agree well with the literature [36]. The positions of conduction band and valance band for semiconductor can be obtained from flat band potentials and some physical properties such as the carrier effective mass and acceptor or donor impurity concentration for semiconductor. The carrier effective mass of $AgIn_5S_8$ is $0.2m_0$ [34], where m_0 is the mass of electron. The positions of valance band and conduction band for the samples determined by the measurement of transmittance spectra and electrochemical analysis in this study are shown in Table 4. The relationship between the absolute electron potential of an electrode (E^{vacuum}) and the normal hydrogen electrode potential (E^{NHE}) is expressed as follows:

$$E^{vacuum} = -E^{NHE} - 4.5 \text{ (at 298 K)} \quad (13)$$

where the electron is 0 eV in a vacuum. Fig. 13 illustrates the band positions of samples determined by electrochemical measurement.

3.5. Photocurrent density and quantum efficiency measurement

The photoelectrode, with an active area of 1.0 cm^2 was installed in the two electrodes photoelectrochemical cell for the measurement of photocurrent. The applied potential between the working and counter electrodes was varied from −1.0 to 3.5 V. The K_2SO_3 (0.25 M) + Na_2S (0.35 M) aqueous solution was used as the electrolyte. For the K_2SO_3 (0.25 M) + Na_2S (0.35 M) solution as electrolyte, the following reactions may occur [2]:

$$SO_3{}^{2-} + H_2O \rightarrow SO_4{}^{2-} + H^+ + e^- \quad (14)$$

$$2S^{2-} \rightarrow S_2{}^{2-} + 2e^- \quad (15)$$

$$S_2{}^{2-} + SO_3{}^{2-} \rightarrow S_2O_3{}^{2-} + S^{2-} \quad (16)$$

$$2H_2O + 2e^- \rightarrow H_2 + 2OH^- \quad (17)$$

The photocurrent densities with applied potential in the range between −0.5 and +0.5 V versus a Pt electrode for samples using K_2SO_3 (0.25 M) + Na_2S (0.35 M) aqueous solution as electrolyte are shown in Fig. 14. It is observed that the photocurrent densities of samples were in the range between 0.002 and 0.01 mA/cm^2 with external bias is zero. Fig. 15 shows the photocurrent densities for the samples prepared in this work with the applied potentials in the range between −1.0 and 3.5 V versus a Pt electrode. All of these samples have the photo-enhancement effect. It is observed that the photocurrent densities of samples e and f reach to 6.0 and 5.94 mA/cm^2 at the external potential 3.5 V, respectively. The photocurrent densities of these samples were in the order e > f > d > c > b > a, while the carrier densities of semiconductors were in the same trends. This may be due to the higher carrier density of samples, the more free electrons taking part in the photochemical process. The carrier density of

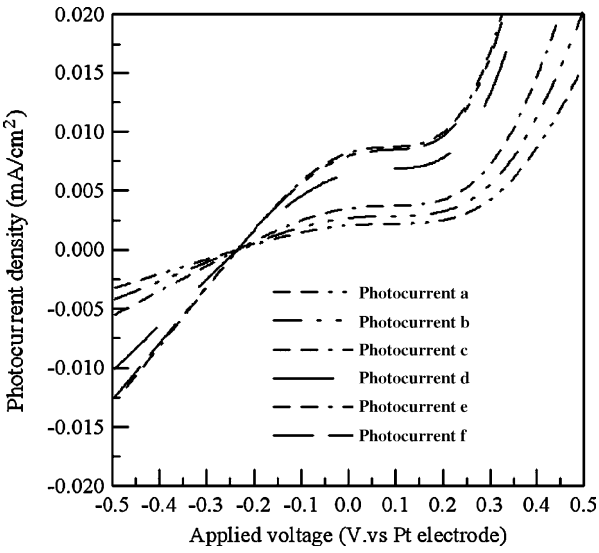

Fig. 14. Photocurrent density–applied voltage plot in the range from −0.5 to 0.5 V for samples at K_2SO_3 (0.25 M) + Na_2S (0.35M) aqueous solution.

$AgIn_5S_8$ polycrystalline film seems to be an important factor for photocurrent of the photoelectrodes. The calculation of quantum efficiency under monochromatic light illumination, $\eta(\lambda)$, can be carried out using the following equation [35]:

$$\eta(\lambda) = \frac{j_p(\lambda)}{eI((\lambda)} \tag{18}$$

where $j_p(\lambda)$ is monochromatic photocurrent density (in mA/cm^2), e the electronic charge, $I(\lambda)$ the flux of incident photons at wavelength λ and λ is the wavelength (in nm), respectively.

A two-electrode system with working electrode and counter electrode was employed for the determination of quantum efficiency of samples e and f prepared in this study. The K_2SO_3 (0.25 M) + Na_2S (0.35 M) aqueous solution was used as electrolyte. Fig. 16 shows the quantum efficiency versus wavelength for samples e and f, ranging from 380 to 900 nm. The quantum efficiency of samples e and f were found out to be 2.2% and 1.7% with the wavelength of incident light at 400 nm and unbiased condition. The onset of the photoelectrochemical response of samples e and f located around 750 nm, corresponding to band-gaps around 1.65 eV, which is closely consistent with the value of band-gaps presented in Table 2 and absorption spectra of samples shown in Fig. 7.

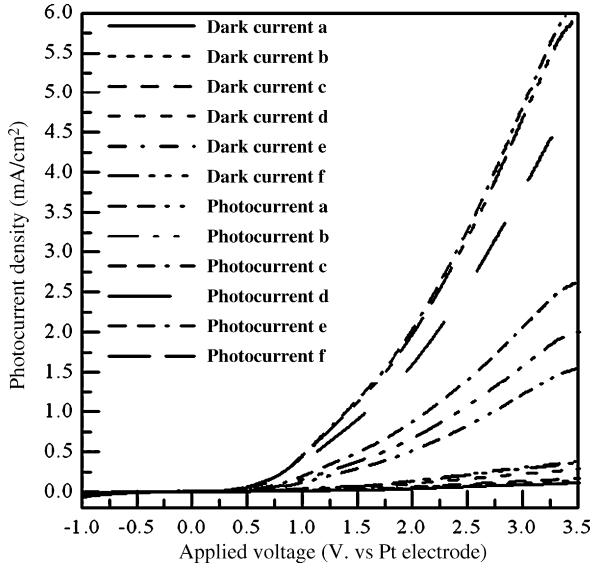

Fig. 15. Photocurrent density–applied voltage plot in th range from −1 to 3.5 V for samples at K_2SO_3 (0.25M) + Na_2S (0.35 M) aqueous solution.

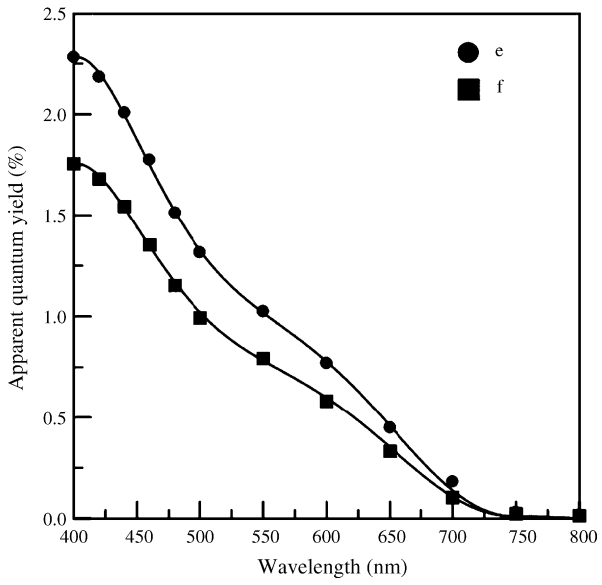

Fig. 16. Plot of quantum efficiency vs. wavelength of incident light for samples e and f at K_2SO_3 (0.25 M) + Na_2S (0.35 M) aqueous solution.

4. Conclusions

In this study, the $AgIn_5S_8$ films were successfully deposited on ITO-coated glass substrates. Metal precursor including Ag^+, In^{3+} was kept at the molar ratio of 1:1. Thioacetamide provide S^{2-} in the acidic solution. The structures, electrical and optical properties of $AgIn_5S_8$ films using chemical bath deposition were investigated to evaluate the possibility of $AgIn_5S_8$ photoelectrodes for photoelectrochemical applications. The XRD patterns show $AgIn_5S_8$ phase is the major crystal structure in this study. With different substrates, the different crystal structures were observed on these films. The maximum photocurrent density of samples in this study was found to be 6.0 mA/cm^2 under the illumination using a 300 Xe lamp system with light intensity set at 100 mW/cm^2. The maximum quantum efficiency of films was found to be 2.2% with wavelength at 400 nm. The band gaps and carrier densities of these samples are lied in the range 1.73 to 1.70 eV, and 4.02 to 6.36×10^{14} cm^{-3}, respectively. The flat band potentials of these samples are in the range of −0.293 to −0.403 V versus normal hydrogen electrode. For the information of these results, the $AgIn_5S_8$ polycrystalline film deposited on ITO-coated glass using chemical bath deposition is suitable for the applications of hydrogen production with solar light.

Acknowledgements

The authors are grateful to National Science Council (Grant No. NSC 95-2218-E-182-003-MY2, NSC 94-2745-E-168-003-URD) and the Bureau of Energy, Ministry of Economic Affairs for support this study.

References

[1] A. Fujishima, K. Honda, Nature 238 (1972) 37–38.
[2] H. Kato, A. Kudo, J. Phys. Chem. B 106 (2002) 5029–5034.
[3] T. Ishii, H. Kato, A. Kudo, J. Photoch. Photobio. A 163 (2004) 181–186.
[4] A. Kudo, M. Sekizawa, Catal. Lett. 58 (1999) 241–243.
[5] A. Kudo, M. Sekizawa, Chem. Commum. (2000) 1371–1372.
[6] S.M. Sze, Physics of Semiconductor Devices, John Wiley & Sons, New York, 1981.
[7] T. Negami, T. Satoh, Y. Hashimoto, S. Shimakawa, S. Hayashi, M. Muro, H. Inoue, M. Kitagawa, Thin Solid Films 403–404 (2002) 197–203.
[8] M.L. Albor Aquilera, J. Aquilar Hernandez, M. Orteqa-Lopez, V.M. Sanchez, M.A. Gonzalez Trujillo, Mat. Sci. Eng. B 102 (2003) 380–384.
[9] A.N. Tiwari, S. Blunier, M. Filzmoser, H. Zogg, D. Schmid, H.W. Schock, Appl. Phys. Lett. 65 (1994) 3347–3349.
[10] I. Tsuji, H. Kato, H. Kobayashi, A. Kudo, J. Am. Chem. Soc. 126 (2004) 13406–13413.
[11] I. Tsuji, H. Kato, A. Kudo (Eds.), Angew. Chem. Int. 44 (2005) 3565–3568.
[12] S. Gall, N. Barreau, S. Harel, J.C. Bernede, J. Kessler, Thin Solid Films 480–481 (2005) 138–141.
[13] Y.B. He, A. Polity, H.R. Alves, I. Osterreicher, W. Kriegseis, D. Pfisterer, B.K. Meyer, M. Hardt, Thin Solid Films 403–404 (2002) 62–65.
[14] K. Muller, S. Milko, D. Schmeiber, Thin Solid Films 431–432 (2003) 312–316.
[15] S.D. Sartale, B.R. Sankapal, M. Lux-Steiner, A. Ennaoui, Thin Solid Films 480–481 (2005) 168–172.
[16] R.S. Mane, B.R. Sankapal, C.D. Lokhande, Thin Solid Films 353 (1999) 29–32.
[17] R.S. Mane, V.V. Todkar, C.D. Lokhande, Appl. Surf. Sci. 227 (2004) 48–55.
[18] Y. Gao, K. Koumoto, Crystal Growth Des. 5 (2005) 1983–2017.
[19] R. Kwok, XPSPEAK 4.1, http://www.phy.cuhk.edu.hk/~surface/XPSPEAK/.
[20] JCPDS No. 00-055-0487, Powder Diffraction File, Joint Committee on Powder Diffraction Standards, ASTM, Newtown Square, PA, USA, 1999.
[21] JCPDS No. 25-1329, Powder Diffraction File, Joint Committee on Powder Diffraction Standards, ASTM, Newtown Square, PA, USA, 1999.
[22] R.S. Mane, C.D. Lokhand, Mater. Chem. Phys. 65 (2000) 1–31.
[23] M. Ghanashyam Krishna, J.S. Piller, A.K. Bhattacharya, Thin Solid Films 357 (1999) 218–222.
[24] R. Swanepoel, J. Phys. E Sci. Instrum. 16 (1983) 1214–1222.
[25] S. Aglian, D. Mangalaraj, Sa.K. Narayandass, G. Mohan Rao, Phys. B. 365 (2005) 93–101.
[26] A.R. Forouhi, I. Bloomer, Phys. Rev. 34 (1986) 7018–7026.
[27] M. Ortega-Lopez, A. Morales-Acevvdo, O. Solorza-Feria, Thin Solid Films 385 (2001) 120–125.
[28] I. Konovalov, L. Makhova, R. Hesse, R. Szargan, Thin Solid Films 493 (2005) 282–287.
[29] I.V. Bodnar, V.F. Gremenok, Thin Solid Films 487 (2005) 31–34.
[30] N.S. Orlova, I.V. Bondar, E.A. Kudritskaya, Cryst. Res. Technol. 33 (1998) 37–42.
[31] K. Yamaguchi, T. Yoshida, D. Lincot, H. Minoura, J. Phys. Chem. B 107 (2003) 387–397.
[32] R. Zhai, S. Wang, H. Xu, H. Wang, H. Yan, Mater. Lett. 59 (2005) 1497–1501.
[33] M. Kostoglou, N. Andritsos, A.J. Karabelas, J. Colloid Interf. Sci. 263 (2003) 177–189.
[34] A.F. Qasrawi, N.M. Gasanly, Cryst. Res. Technol. 36 (2001) 457–464.
[35] J. Akikusa, S.U.M. Khan, Int. J. Hydro. Eng. 22 (1997) 875–882.
[36] L. Makhova, R. Szargan, I. Konovalov, Thin Solid Films 472 (2005) 157–163.